Available online at www.sciencedirect.com

ScienceDirect

Procedia Engineering 171 (2017) 836 – 846

Procedia Engineering

www.elsevier.com/locate/procedia

Sustainable Civil Engineering Structures and Construction Materials, SCESCM 2016

Numerical approximation of acoustic equation using radial basis function-discontinuous Galerkin method

Kresno W.S.[a,*], S.P.R. Wardani[a], Endra Susila[b], Pranowo[c]

[a]*Civil Engineering Faculty, Diponegoro University, Semarang, Indonesia*
[b]*Civil and Environmental Engineering Faculty, Bandung Institute of Technology, Bandung, Indonesia*
[c]*Informatics Department, Atmajaya University, Yogyakarta, Indonesia*

Abstract

Acoustic equation is an important equation in order to determine wave propagation in a medium. The Application of acoustic equations vastly known, i.e. elastic wave propagation, fluid dynamics and gas dynamics equivalent. This paper present *Radial Basis Function-Discontinuous Galerkin Method* (RBF-DGM) in order to solve acoustic equation. RBF-DGM method is a numerical method, proposed to solve partial differential equations (PDE). RBF-DGM approximated the space domain with RBF and using DGM for time integration method. RBF-DGM application presented then in order to solve acoustic equation. The numerical of RBF-DGM presented, and compared with analytical solution as a result. The numerical results, show that the RBF-DGM (linear) predicting the exact results or analytical well.

Peer-review under responsibility of the organizing committee of SCESCM 2016.

Keywords: RadialBasis Function; Discontinuous Galerkin Method; Numerical Method; Acoustic wave

1. Introduction

Acoustic equation is an important equation in order to determine wave propagation in a medium. The form itself is a second order of partial differential equation (PDE). The Application of acoustic equations vastly known, i.e. elastic wave propagation, fluid dynamics and gas dynamics equivalent [1]. In some case, the acoustic equation has analytical or exact solution, but in fact, analytical solutions not easily found in daily life, so the numerical method is

* Corresponding author.
E-mail address: kresnowikan@gmail.com

Peer-review under responsibility of the organizing committee of SCESCM 2016.
doi:10.1016/j.proeng.2017.01.375

the main tool to solve these equations. Recently the mesh-based numerical methods that require the creation of grid or mesh is a popular method and has developed well. Some alternative numerical method that is not based on a mesh or mesh-less or mesh-free lately gained popularity but still in the early stages and is very open for further research. Numerical methods based on creating mesh, for example Finite Difference Method (FDM), Finite Element Method (FEM) and Finite Volume Method (FVM). Examples of meshfree methods are Element Free Galerkin (EFG), Reproducing Kernel Particle Method (RKPM), Smoothed Particle Hydrodynamics (SPH), Radial Basis Function (RBF). Meshless method has the advantage compared to the mesh-based method, which does not require the creation of mesh on the domain, thus making meshless method to be simpler. In addition meshless method is suitable in problems involving changes in the geometry domain, because it does not need an effort mesh back (remeshing) on the domain.

FDM method is a method based on grid or mesh-based numerical method. This method is simple, the earliest used, and is still used in many different areas of science and engineering recently. This method is simple, because it is formulated directly from the calculus [2]. FDM method can be used directly on the governing equations of a problem. Otherwise, difficulties found in order to solve problems with complex geometries and boundaries.

FEM in the other hand, a numerical method using variation methods or the weighted residual method (MWR) to create weakform of governing equations. Weakform subsequently used to approximate the existing problem. FEM method based on sub domains or elements on the domain, so the method is included in the mesh-based method [3]. This method has the advantage compared to the FDM to solve complex geometry. This method is very widely applied in various fields of science and engineering. Lately discontinuous Galerkin Method (DGM) introduced, this method is derived from FEM. DGM method has the advantage that the higher order accuracy, *hp*-adaptivity, has semidiscrete scheme and has a good performance for the simulation that has discontinuity [4].

FVM method, a grid based method that divides the domain into a cell and the integration is performed on each cell. Integration performed on each cell for evaluation flux entering and leaving the cell, as a conserve quantity. This method is very popular in computational fluid dynamics (CFD).

EFG method is a meshless method, which uses a weak form of the governing equations and moving least square (MLS) in the shape function [5]. EFG method offers the ability to create domain without mesh of domain. EFG method offers the ability to solve the problem without creating a mesh of domain. Background mesh is still required to perform the integration of the weak form. Application of the EFG is a problem of elastostatic and propagation crack.

RBF method firstly applied to solve the data interpolation on scattered data. RBF has also applied in solving PDE numerically. RBF is a numerical method based on meshless using collocation principles on governing equations. The advantages of RBF is accurate, simple and truly meshless, without using background mesh. RBF produce a high condition number of and full system matrix [6].

Numerical solution of the time domain is very important in order to get an accurate response of the model. Generally, integration worked with explicit fourth order of Runge Kutta method, Newmark-β, HHT- α, Wilson-θ etc [7]. Some numerical methods based or grid-based mesh combined with time integration to solve the problem of PDE numerically on the space and time domain. Explicit methods generally require time increment, Δt is small enough, such that a stable simulation achieved. By using a small Δt conductlong enough simulation or long runtime. Therefore, faster and more stable integration time required to solve with, for example implicit method. One of the implicit methods for the integration time is DGM.

This paper presented numerically solving acoustic equation. Solving conducted by combining the method of RBF and DGM. Completion conducted by combining the method of RBF and DGM, well known as RBF-DGM, combining both methods with partial discretization [3]. The RBF method for solving the space domain used is for the ease and accuracy reason. Time integration are selected using DGM because of implicit and stability behavior. Combining these two methods produce a simple, accurate and stable calculation.

2. Method

Acoustic equation in two dimensions shown in Eq. 1, where p is the independent variable that will be calculated, c is a constant, t time and x, y space domain.

$$\frac{\partial^2 p(x,y,t)}{\partial t^2} - c^2\left(\frac{\partial^2 p(x,y,t)}{\partial x^2} + \frac{\partial^2 p(x,y,t)}{\partial y^2}\right) = 0 \tag{1}$$

Initial condition for acoustic equation shown in Eq. 2, where $x_0$and y_0 is the origin of the exponential function and A is a constant.

$$p(x,y,0) = \exp(-A(x-x_0)^2 + (y-y_0)^2) \tag{2}$$

Analytic solution of Eq. 1 and Eq. 2, shown in Eq. 3 [8].

$$p = \frac{1}{2A}\int_0^\infty \left(\cos(\lambda t) - \frac{\beta}{2A}\lambda \sin(\lambda t)\right) \lambda J_0(\lambda r) e^{-\frac{\lambda^2}{2A}}\, \mathrm{d}\lambda \tag{3}$$

where J_0 is Bessel function of the first kind of first order and r expressed in Eq. 4, and β a constant equal to 0.04.

$$r = \sqrt{(x-Mt)^2 + y^2} \tag{4}$$

The following are solving the acoustic equation in Eq. 1 with RBF-DGM. By simplifying Eq.1 into Eq. 5.

$$\frac{\partial^2 p}{\partial t^2} - c^2 \mathcal{L}(p(x,y,t)) = 0 \tag{5}$$

Where, differential operator $\mathcal{L}$ is expressed in Eq. 6.

$$\mathcal{L}(\quad) = \frac{\partial^2(\quad)}{\partial x^2} + \frac{\partial^2(\quad)}{\partial y^2} \tag{6}$$

Eq. 6 converted into two first-order ordinary differential equation (ODE). Eq. 1 is converted into two ODE of first order shown in Eq. 7a and 7b.

$$\frac{\partial u}{\partial t} = c^2 \mathcal{L}\big(p(x,y,t)\big) \tag{7a}$$

$$\frac{\partial p}{\partial t} = u \tag{7b}$$

Eq. 7a and 7b approximated by Radial Basis Function (RBF), expressed in Eq. 8. Where, *N* is the number of nodes on the domain and boundary.

$$p(\mathbf{r},t) \cong \hat{p}(\mathbf{r},t) \cong \sum_{j=1}^{N} \alpha_{(p)j}(t)\, \phi\big(\|\mathbf{r}_i - \mathbf{r}_j\|\big) \text{ for } \quad i = 1,2,..,N \tag{8}$$

The value of $\phi\big(\|\mathbf{r}_i - \mathbf{r}_j\|\big)$ is radial basis function, which depends on the distance between each node. The value of $\mathbf{r}_i$ is the position of node i, the position of center node expressed by $\mathbf{r}_j$, where $\mathbf{r}_i = x_i\mathbf{i} + y_i\mathbf{j}$ and $\mathbf{r}_j = x_j\mathbf{i} + y_j\mathbf{j}$. The distance between node i and the center node j showed in Eq. 9. Fig. 1 shows the distance between nodes in a domain with nodes distributed randomly. Radial basis function using multiquadratic function expressed in Eq. 10 where s is the shape parameter and l is the distance of each node [6].

$$l = \sqrt{\left(x_j - x_i\right)^2 + \left(y_j - y_i\right)^2} \tag{9}$$

$$\phi = \sqrt{1 + (ls)^2} \tag{10}$$

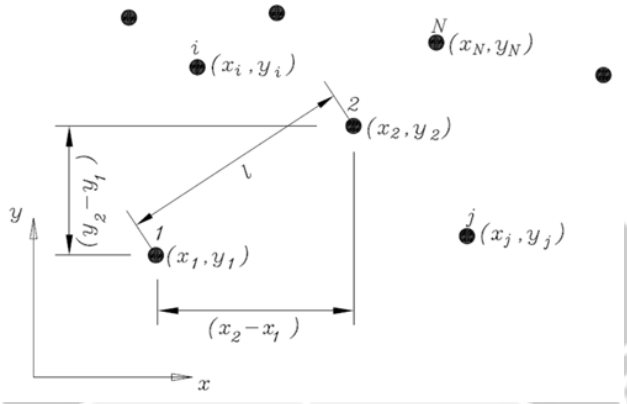

Fig. 1. Distribution of the node and the distance between nodes

Value $\alpha_{(u)j}(t)$ and $\alpha_{(p)j}(t)$ in Eq. 8a and 8b are parameters which are calculated in such a way to produce an appropriate value. By substituting Eq. 8a and 8b to Eq. 7a and 7b resulted in Eq. 11. Where p_i and u_i are p and u in the node i.

$$\frac{\partial u_i}{\partial t} - c^2 \mathcal{L}\left(\sum_{j=1}^{N} \alpha_{(p)j}(t)\, \phi\left(\|\boldsymbol{r}_i - \boldsymbol{r}_j\|\right)\right) = 0 \qquad \text{for } \; i = 1,2,..,N \tag{11a}$$

$$\frac{\partial p_i}{\partial t} - u = 0 \quad \text{for } \; i = 1,2,..,N \tag{11b}$$

With matrix notation then Eq. 11a and 11b can be expressed in Eq. 12a and 12b.

$$\frac{\partial \mathbf{u}}{\partial t} - c^2 \mathcal{L}\mathbf{B}\boldsymbol{\alpha}_{(p)} = 0 \tag{12a}$$

$$\frac{\partial \mathbf{p}}{\partial t} - \mathbf{u} = 0 \tag{12b}$$

By inversion in Eq. 8 to obtain $\alpha_{(p)j}(t)$, and back substitution to the Eq. 12a and 12b, and multiply all term with matrix **B** then produce Eq. 13a and 13b.

$$\mathbf{B}\frac{\partial \mathbf{u}}{\partial t} - c^2 \mathbf{H}\mathbf{p} = 0 \tag{13a}$$

$$\mathbf{B}\frac{\partial \mathbf{p}}{\partial t} - \mathbf{B}\mathbf{u} = 0 \tag{13b}$$

where

$$\mathbf{u} = \begin{pmatrix} u_1 \\ u_2 \\ \vdots \\ u_N \end{pmatrix}; \qquad \mathbf{p} = \begin{pmatrix} p_1 \\ p_2 \\ \vdots \\ p_N \end{pmatrix}; \qquad \mathbf{B} = \sum_{j=1}^{N} \phi\left(\|\mathbf{r}_i - \mathbf{r}_j\|\right); \qquad \mathbf{H} = \mathcal{L}\left(\sum_{j=1}^{N} \phi\left(\|\mathbf{r}_i - \mathbf{r}_j\|\right)\right) \text{for } \; i = 1,2,..,N \tag{14}$$

Matrix **u** and **p** is the column matrix of $N\times1$ elements. Matrix **B** and **H** is matrix that has $N\times N$ elements. Matrix **B** contains elements of radial basis function where each element calculated by finding the distance between each node and substituting in Eq. 10. Matrix **H** in Eq. 13 and 14 contains space derivatives of radial basis function at each node, calculated from Eq. 15, 16 and 17.

$$\mathcal{L}(\phi) = \frac{\partial^2(\phi)}{\partial x^2} + \frac{\partial^2(\phi)}{\partial y^2} \tag{15}$$

where

$$\frac{\partial^2\phi}{\partial x^2} = \frac{\mathrm{d}\phi}{\mathrm{d}l}\frac{\partial^2 l}{\partial x^2} + \frac{\mathrm{d}^2\phi}{\mathrm{d}l^2}\left(\frac{\partial l}{\partial x}\right)^2 ; \frac{\partial^2\phi}{\partial y^2} = \frac{\mathrm{d}\phi}{\mathrm{d}l}\frac{\partial^2 l}{\partial y^2} + \frac{\mathrm{d}^2\phi}{\mathrm{d}l^2}\left(\frac{\partial l}{\partial y}\right)^2 \tag{16}$$

and

$$\frac{\partial l}{\partial x} = \frac{x}{l} ; \quad \frac{\partial^2 l}{\partial x^2} = \frac{1-\left(\frac{\partial l}{\partial x}\right)^2}{l} ; \quad \frac{\partial l}{\partial y} = \frac{y}{l} ; \quad \frac{\partial^2 l}{\partial y^2} = \frac{1-\left(\frac{\partial l}{\partial y}\right)^2}{l} \tag{17a}$$

$$\frac{\mathrm{d}\phi}{\mathrm{d}l} = \frac{s^2 l}{\sqrt{1+s^2 l^2}} \quad ; \quad \frac{\mathrm{d}^2\phi}{\mathrm{d}l^2} = \frac{s^2}{(1+s^2 l^2)^{3/2}} \tag{17b}$$

Eq. 13a and 13b is a system of ODE, result from acoustic equation with RBF approach. The ODE solved with time integration from DGM. The process of solving performed as follows. The time domain is divided into subintervals $I_n = [t_n, t_{n+1}]$, where $n = 0,1,\ldots,M-1$. The value of **p** and **u** approximated by $\hat{\mathbf{p}}$ and $\hat{\mathbf{u}}$ shown in Eq. 18. Where $\phi_1(\xi)$ and $\phi_2(\xi)$ is a linear shape function in natural coordinates ξ, expressed in Eq. 19.

$$\hat{\mathbf{u}} = \hat{\mathbf{u}}_n^+\phi_1(\xi) + \hat{\mathbf{u}}_{n+1}^-\phi_2(\xi) \quad ; \quad \hat{\mathbf{p}} = \hat{\mathbf{p}}_n^+\phi_1(\xi) + \hat{\mathbf{p}}_{n+1}^-\phi_2(\xi) \tag{18}$$

where

$$\phi_1(\xi(t)) = \frac{1}{2}(1-\xi(t)) \quad ; \quad \phi_2(\xi) = \frac{1}{2}(1+\xi(t)) \tag{19}$$

Time integration with DGM processes done by multiplying the DE with test function and integrates on a subdomain [4, 9]. Approximation value, $\hat{\mathbf{p}}$ and $\hat{\mathbf{u}}$ substitute in Eq. 13a and 13b and multiplied by a test function equal to shape function ϕ_l in Eq. 19 then produces Eq. 20a and 20b.

$$\int_{t_n}^{t_{n+1}} \left(\phi_l \mathbf{B}\frac{\partial \mathbf{u}}{\partial t} - \phi_l c^2 \mathbf{H}\mathbf{p}\right)\mathrm{d}t = 0 \qquad \text{for } \phi_l = \phi_1, \phi_2 \tag{20a}$$

$$\int_{t_n}^{t_{n+1}} \left(\phi_l \mathbf{B}\frac{\partial \mathbf{p}}{\partial t} - \phi_l \mathbf{B}\mathbf{u}\right)\mathrm{d}t = 0 \qquad \text{for } \phi_l = \phi_1, \phi_2 \tag{20b}$$

Eq. 20a and 20b carried out integration by parts twice and transformed the natural coordinate ξ and for $\phi_l = \phi_1$ Eq. 20a and 20b become Eq. 21a and 21b.

$$\phi_1(t_n^+)\mathbf{B}\hat{\mathbf{u}}(t_n^+) - \phi_1(t_n^-)\mathbf{B}\hat{\mathbf{u}}(t_n^-) + \int_{-1}^{+1}\left(\frac{1}{2}(1-\xi)\mathbf{B}\frac{\partial\hat{\mathbf{u}}}{\partial t} - \frac{1}{2}(1-\xi)c^2\mathbf{H}\hat{\mathbf{p}}\right)\frac{\Delta t}{2}\mathrm{d}\xi = 0 \tag{21a}$$

$$\phi_1(t_n^+)\mathbf{B}\hat{\mathbf{p}}(t_n^+) - \phi_1(t_n^-)\mathbf{B}\hat{\mathbf{p}}(t_n^-) + \int_{-1}^{+1}\left(\frac{1}{2}(1-\xi)\mathbf{B}\frac{\partial\hat{\mathbf{p}}}{\partial t} + \frac{1}{2}(1-\xi)\mathbf{B}\hat{\mathbf{u}}\right)\frac{\Delta t}{2}\mathrm{d}\xi = 0 \quad (21b)$$

Similar to $\phi_l = \phi_2$, then Eq. 20a and 20b become Eq. 22a and 22b

$$\phi_2(t_n^+)\mathbf{B}\mathbf{u}(t_n^+) - \phi_2(t_n^-)\mathbf{B}\mathbf{u}(t_n^-) + \int_{-1}^{+1}\left(\left(\frac{1}{2}(1-\xi)\mathbf{B}\right)\frac{\partial\hat{\mathbf{u}}(t)}{\partial t} - \left(\frac{1}{2}(1-\xi)\right)c\mathbf{H}\hat{\mathbf{p}}\right)\frac{\Delta t}{2}\mathrm{d}\xi = 0 \quad (22a)$$

$$\phi_2(t_n^+)\mathbf{B}\mathbf{p}(t_n^+) - \phi_2(t_n^-)\mathbf{B}\mathbf{p}(t_n^-) + \int_{-1}^{+1}\left(\left(\frac{1}{2}(1-\xi)\mathbf{B}\right)\frac{\partial\hat{\mathbf{p}}(t)}{\partial t} + \left(\frac{1}{2}(1-\xi)\right)\mathbf{B}\hat{\mathbf{u}}\right)\frac{\Delta t}{2}\mathrm{d}\xi = 0 \quad (22b)$$

According Eq. 19, $\phi_1(t_n^+) = 1$, $\phi_2(t_n^-) = 1$, $\phi_2(t_n^+) = 0$, $\phi_2(t_n^-) = 0$ and for simplicity $\hat{\mathbf{u}}(t_n^+) = \hat{\mathbf{u}}_n^+$; $\hat{\mathbf{u}}(t_n^-) = \hat{\mathbf{u}}_n^-$; $\hat{\mathbf{p}}(t_n^+) = \hat{\mathbf{p}}_n^+$ and $\hat{\mathbf{p}}(t_n^-) = \hat{\mathbf{p}}_n^-$, then Eq. 21a, 21b, 22a and 22b can be written in matrix form in Eq. 23. In Eq. 23, that the matrix system which is the first term produces degree of freedom, d.o.f., twice the number of independent variables (**u** and **p**).

$$\begin{pmatrix} -\frac{1}{3}c^2\Delta t\,\mathbf{H} & -\frac{1}{6}c^2\Delta t\,\mathbf{H} & \frac{1}{2}\mathbf{B} & \frac{1}{2}\mathbf{B} \\ \frac{1}{2}\mathbf{B} & \frac{1}{2}\mathbf{B} & -\frac{1}{3}\Delta t\mathbf{B} & -\frac{1}{6}\Delta t\mathbf{B} \\ -\frac{1}{6}c^2\Delta t\,\mathbf{H} & -\frac{1}{3}c^2\Delta t\,\mathbf{H} & -\frac{1}{2}\mathbf{B} & +\frac{1}{2}\mathbf{B} \\ -\frac{1}{2}\mathbf{B} & \frac{1}{2}\mathbf{B} & -\frac{1}{6}\Delta t\mathbf{B} & -\frac{1}{3}\Delta t\mathbf{B} \end{pmatrix}\begin{pmatrix} \hat{\mathbf{u}}_n^+ \\ \hat{\mathbf{u}}_{n+1}^- \\ \hat{\mathbf{p}}_n^+ \\ \hat{\mathbf{p}}_{n+1}^- \end{pmatrix} = \begin{pmatrix} \mathbf{B}\hat{\mathbf{u}}_n^- \\ \mathbf{B}\hat{\mathbf{p}}_n^- \\ 0 \\ 0 \end{pmatrix} \quad (23)$$

Calculation $\hat{\mathbf{u}}$ and $\hat{\mathbf{p}}$ value is done for each subintervals $I_n = [t_n, t_{n+1}]$ according to the Eq. 23. The following describes the calculation steps. The domain is determined first, then the node distributed in the domain. From the distribution node can be determined the distances between nodes l, with Eq. 9. The value of ϕ or $\phi\left(\|\mathbf{r}_i - \mathbf{r}_j\|\right)$ for each node determined by the distance of each node by using Eq. 10. By knowing the value $\phi\left(\|\mathbf{r}_i - \mathbf{r}_j\|\right)$ then the matrix **B** calculated. The matrix **H** can be calculated from Eq 15,16 and 17 a and 17b. After calculating the matrix **B** and **H**, the system matrix, which is the first term of left hand side (RHS) in Eq. 23 can be calculated.

The following describes the steps to calculate the unknown value (**u** and **p**), using Eq. 23. The initial value or initial condition of Eq. 2 can be used to calculate $\mathbf{B}\hat{\mathbf{u}}_n^-$ and $\mathbf{B}\hat{\mathbf{p}}_n^-$ for $n = 1$ or $(\mathbf{B}\hat{\mathbf{p}}_1^-)$ in Eq. 23, corresponding to $\mathbf{B}\hat{\mathbf{p}}^-(t = 0)$. By knowing $\mathbf{B}\hat{\mathbf{u}}_n^-$ and $\mathbf{B}\hat{\mathbf{p}}_n^-$, the right hand side (RHS) Eq. 23 can be determined. By knowing RHS Eq. 23, then the second term on the LHS of Eq. 23 can be determined, by inversion Eq. 23. So that $(\hat{\mathbf{u}}_n^+ \;\; \hat{\mathbf{u}}_{n+1}^- \;\; \hat{\mathbf{p}}_n^+ \;\; \hat{\mathbf{p}}_{n+1}^-)^T$ for $n = 1$ or $(\hat{\mathbf{u}}_1^+ \;\; \hat{\mathbf{u}}_2^- \;\; \hat{\mathbf{p}}_1^+ \;\; \hat{\mathbf{p}}_2^-)^T$ in Eq. 23 can be determined. So that $\hat{\mathbf{u}}_2^-$ and $\hat{\mathbf{p}}_2^-$ corresponding to $t = \Delta t$, or $\hat{\mathbf{u}}^-(t = \Delta t)$ and $\hat{\mathbf{p}}^-(t = \Delta t)$can be determined. Values $\hat{\mathbf{u}}_2^-$ and $\hat{\mathbf{p}}_2^-$are then used as an initial condition for calculating $(\hat{\mathbf{u}}_2^+ \;\; \hat{\mathbf{u}}_3^- \;\; \hat{\mathbf{p}}_2^+ \;\; \hat{\mathbf{p}}_3^-)^T$, so the value of the $\hat{\mathbf{u}}_3^-$ and $\hat{\mathbf{p}}_3^-$corresponding to $t = 2\Delta t$ or $\hat{\mathbf{u}}_3^-(t = 2\Delta t)$ and $\hat{\mathbf{p}}_3^-(t = 2\Delta t)$, can be calculated. The process above can be looping until $\hat{\mathbf{u}}_{n+1}^-$ and $\hat{\mathbf{p}}_{n+1}^-$produces value corresponding to the final time t_f or $\hat{\mathbf{u}}^-(t = t_f)$ and $\hat{\mathbf{p}}^-(t = t_f)$.

3. Numerical Tests

The following are the steps of numerical test for acoustic equation by RBF-DGM, with the steps described above. Numerical simulations, performed on a square domain. Domain has a length and width of 30. Initial condition, for acoustic equation in the form of the exponential function expressed in Eq. 2. The center of the exponential function in Eq. 2 on the coordinate (0.0; 0.0) is shown in Fig. 2 as a black node, so $x_0 = 0$ and $y_0 = 0$, in Eq. 2. The coefficient of the exponential function is set to $A = \frac{\log(2)}{9}$, in Eq. 2. The first signal receiver (rec. 1) at coordinates (5;

0) and the second signal receiver (rec. 2) at coordinates (10; 0). The first and second signal receiver is shown as a green nodes on the right side of the center is shown in Fig. 2.

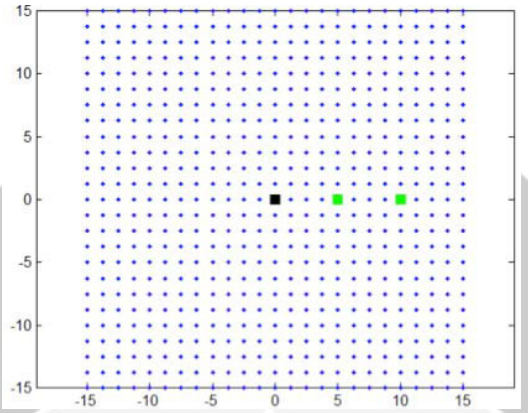

Fig. 2. Distribution of 25^2 nodes, distributed evenly to the domain. First receiver located at the green node (5,0). Second receiver located at green node (10,0)

Distribution node on the domain, using 25^2 nodes, shown in Fig. 2. The simulation beginning at time 0, and the final time is 8. Analytical solutions and numerical results by RBF-DGN (*linear* DGM) is shown in Fig. 3, for a time increment of 0.1 ($\Delta t = 0.1$), by 25^2 nodes and shape parameter $s = 1$. Response to the first and second receiver, of unknown variables $\hat{\mathbf{p}}$, compared with analytical results are shown in Fig. 3. In Fig. 3 displays the results of numerical or analytically predict the exact results well. In Fig. 3, show that the numerical prediction has almost the same amplitude with analytical results, both for the first and second receiver. Numerical results predict form of response, which is almost the same, for the first and second receiver. The difference that arises is, the analytical result lagged behind the numerical results. This delay gives numerical difference between the exact and numerical results. The difference shown as $\log_{10}\|p_{\text{exact}} - p_{\text{numerical}}\|_2$.

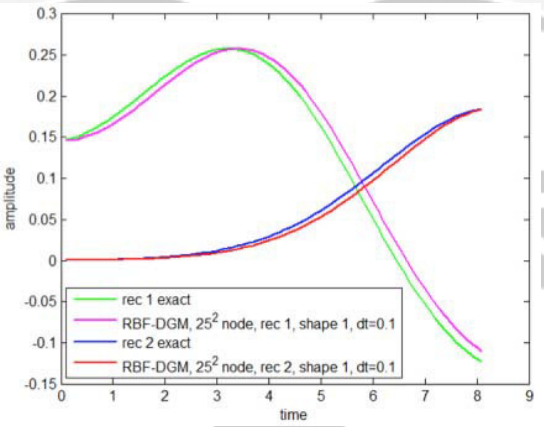

Fig. 3. Response unknown variable $\hat{\mathbf{p}}$ of RBF-DGN (linear DGM) compared to exact results or analytical result for $\Delta t = 0.1; 0.05; 0.01$; 25^2 nodes; shape parameter s = 1

The difference between the numerical results and the exact is expressed as $\log_{10}\|\text{error}\|_2 = \log_{10}\|p_{\text{exact}} - p_{\text{numerical}}\|_2$. For receiver 1 (rec. 1), is shown in Fig. 4 for $\Delta t = 0.1; 0.05; 0.01$ and shape parameter $s = 1$. For simplicity, error is $\log_{10}\|\text{error}\|_2 = \log_{10}\|p_{\text{exact}} - p_{\text{numerical}}\|_2$. The error curve for various time increment ($\Delta t =$

$0.1; 0.05; 0.01$) at rec. 1, is coincide, such as a single curve. Error value, fluctuating forming a concave curve downward, with two peaks.

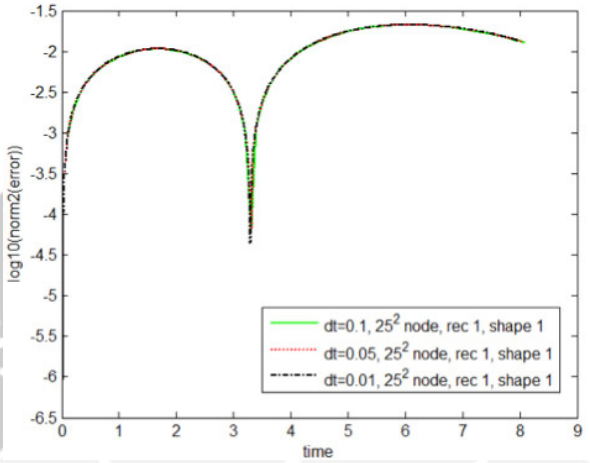

Fig. 4. The time history error for $\Delta t = 0.1; 0.05; 0.01$ for the first receiver (rec. 1) and shape parameter $s = 1$

Error curve for the rec. 2 shown in Fig. 5. In the rec. 2, error curve similar to rec. 1, for the variation of time increment $\Delta t = 0.1; 0.05; 0.01$. In general, from Fig. 4 and Fig. 5 shows that the error peak for the second receiver is smaller than the first one. The rate of increase in error for rec. 1 is lower than the rec. 2, for the shape parameter 1.

Simulations with different parameter values shape also conducted in order to get a picture of error generated. Error of RBF-DGM (DGM linear) for the rec. 1 for various time increments $\Delta t = 0.1;\ 0.05;\ 0.01$ and shape parameter 3, shown in Fig. 6. The error on the rec.2, for $\Delta t = 0.1; 0.05; 0.01$ and shape parameter $s = 3$ is shown in Fig. 7. On a larger shape parameter, time history error will still coincide for various time increments. The rate of increase in error for rec. 1 is lower than the rec. 2, for the shape parameter 3

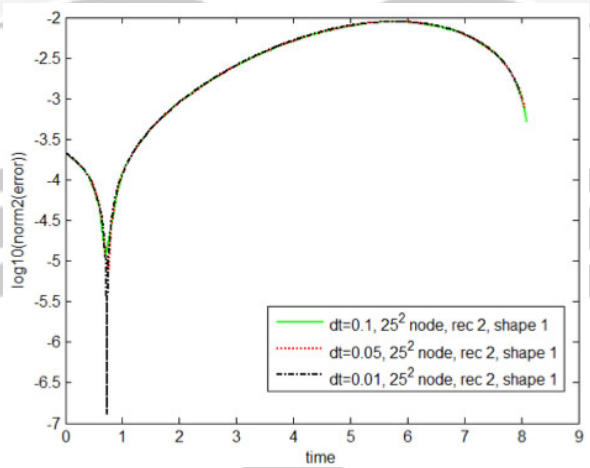

Fig. 5. The time history error for $\Delta t = 0.1; 0.05; 0.01$ for the second receiver (rec. 2) and shape parameter s=1

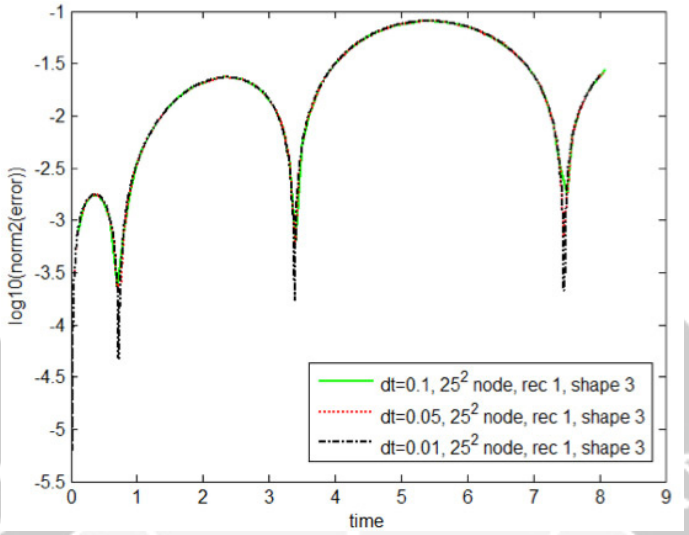

Fig. 6. The time history error for $\Delta t = 0.1; 0.05; 0.01$ for the first receiver (rec. 1) and shape parameter s=3.

The effects of shape parameter variation at time history error, for the rec.1 shown in Fig. 8. In rec. 1, a higher shape parameter, tend to produce higher error, shown in Fig. 8. The results were the same for the second receiver, a shape parameter higher yield higher error, they are shown in Fig. 9. Low values at shape parameter values tend to produce lower error rate. The results of the independent variable at a time 6 seconds is shown in Fig. 10.

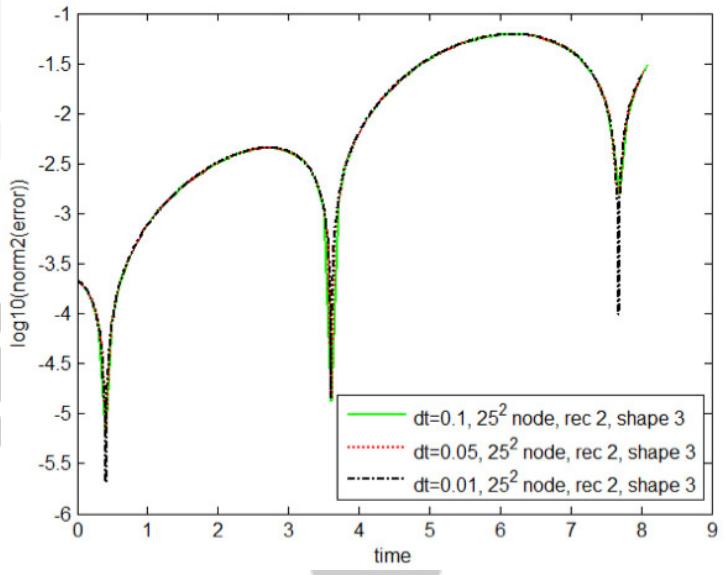

Fig. 7. The time history error for $\Delta t = 0.1; 0.05; 0.01$ for the second receiver (rec. 2) and shape parameter s=3.

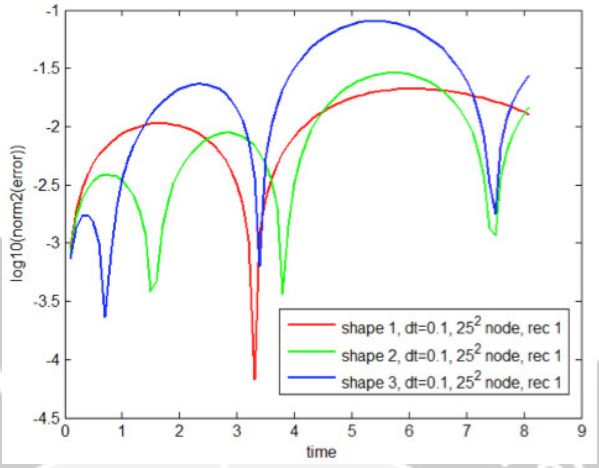

Fig. 8. The time history error for various shape parameter, for $\Delta t = 0.1$ for the first receiver (rec. 1).

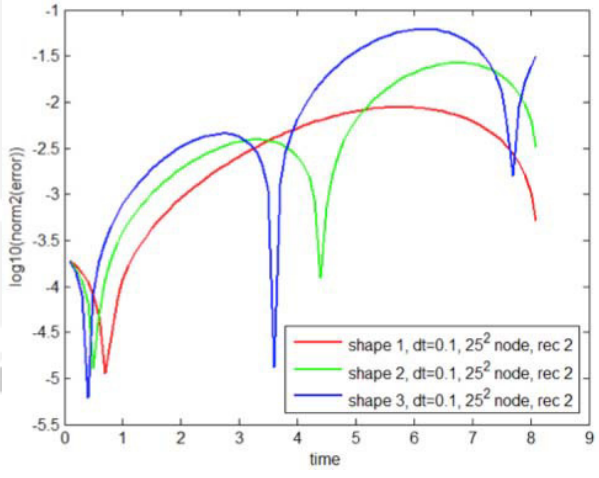

Fig. 9. The time history error for various shape parameter, for $\Delta t = 0.1$ for the second receiver (rec. 2)

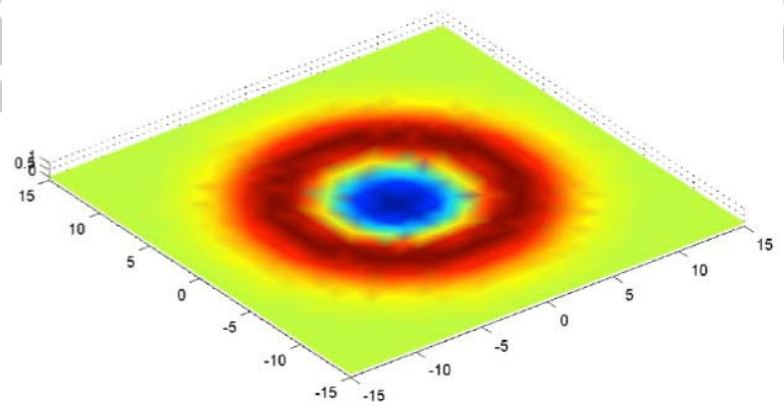

Fig. 10. The response of the independent variable, at 6 seconds

4. Conclusion

The results of numerical tests on acoustic equation; the numerical results, show that the RBF-DGM (linear) predicting the exact results or analytical well. The results of numerical tests show the time increment does not affect on the error. In this scheme, at the time increment is large, resulting in a numerical solution that does not vary much with the small one. Generally, higher value of shape parameter tends to produce higher error rate.

References

[1] R. J. Leveque, Finite volume method for hyperbolic problem, Cambridge University Press, 2002.
[2] K. A. Hoffmann, Computational fluid dynamics vol. 1, Engineering Education System, 2002.
[3] O.C. Zienkiewicz, K. Morgan, Finite element and approximation, John Wiley & Sons, 1982.
[4] J.S. Hesthaven, T. Warburton, Nodal discontinuous Galerkin methods: algorithms, analysis, and applications,Springer, New York, 2008.
[5] T. Belytschko, Y.Y. Liu, L. Gu, Element-free Galerkin method. Int. J. Num. Meth. Eng., 37:229-256,1994.
[6] S.A. Sarra, E.J.Kansa, Multiquadratic radial basis function approximation method for numerical solution of partial differential equations, Tech Science Press, 2010.
[7] K.J. Bathe, Finite element procedures, Prentice Hall, 1996.
[8] C. P. A. Blom, Discontinuous Galerkin method on tetrahedral element for aeroacoustics, Ph.D Thesis, Twente University, 2006.
[9] Ben Q. Li, Discontinuous finite element in fluid and heat transfer, Springer, 2006.